Polymer 50 (2009) 2624–2629

Contents lists available at ScienceDirect

Polymer

journal homepage: www.elsevier.com/locate/polymer

Synthesis and characterization of nanostructured polypyrroles: Morphology-dependent electrochemical responses and chemical deposition of Au nanoparticles

Ping Xu [a,b], Xijiang Han [a,*], Bin Zhang [a], Nathan H. Mack [b], Sea-Ho Jeon [b], Hsing-Lin Wang [b,*]

[a] Chemistry Laboratory Center, Department of Chemistry, Harbin Institute of Technology, Harbin 150001, China
[b] Physical Chemistry and Spectroscopy, Chemistry Division, Los Alamos National Laboratory, Los Alamos, New Mexico 87545, USA

ARTICLE INFO

Article history:
Received 8 December 2008
Received in revised form
3 March 2009
Accepted 7 March 2009
Available online 17 March 2009

Keywords:
Polypyrrole
Nanoparticles
Shape

ABSTRACT

We report here the preparation of nanostructured polypyrroles (PPys) with different morphologies (nanospherical or nanofibrillar) through a surfactant-assisted oxidative polymerization route. Nanofibrillar PPy has a higher redox current, presumably due to a higher surface area accessible to the electrolytes and a lower charge transfer resistance compared to that of the spherical PPy. The impedance spectrum of spherical PPy at lower frequencies suggests a semi-infinite diffusion process, while nanofibrillar PPy displays barrier diffusion and capacitor characteristics. Electrodeless (chemical) deposition of Au particles from $AuCl_4^-$ aqueous solution using nanostructured PPy also shows different morphologies, presumably due to a difference in growth kinetics dominated by the differences in surface area and surface chemistry. Our work demonstrates control over the electrochemical responses and charge transfer mechanisms of these conducting polymers. This control arises from their unique length scale geometries and surface areas that allows for the fabrication of Au nanoparticles with tunable morphologies. Our work in the controlled synthesis of nanostructured conducting polymers and metal nanoparticles opens up new opportunities for nanofiber-based electronic and sensory devices.
© 2009 Elsevier Ltd. All rights reserved.

1. Introduction

There is an increasing interest in the controlled synthesis of nanomaterials with tunable sizes and morphologies as they can play a vital role in determining a material's properties [1–3]. Nanostructured conducting polymers have generated much interest for their potential use in nanoelectronics and organic conductors [4–7]. Polypyrrole (PPy) and polyaniline are promising conducting polymers for commercial applications due to their high conductivity, easy preparation, and environmental stability [8–10]. However, differences between the PPy and polyaniline (PANI) systems lie in the fact that they require different kinds of seed templates to ensure fibrillar polymer growth. It is known that fibrillar growth is intrinsic to PANI, and that an added seed template directs the synthetic trajectory along these pre-existing pathways [11–13]. In the PPy system, however, these pathways have to be induced using either seed templates that are intrinsically reactive toward the pyrrole monomer or those that can be rendered reactive.[11] Otherwise, only spherical PPy is produced [14,15].

In recent years, Virji et al. have shown that PANI nanofibers can be easily prepared and upscaled. They also demonstrated using PANI nanofibers to fabricate highly sensitive chemical sensors [16]. More recently, Tseng et al. fabricated efficient memory devices using these nanofibers with chemically deposited Au nanoparticles that have nanometer length scale and high surface area [17]. The above works demonstrate the importance of having high surface area nanofibers and the significance of having high density Au nanoparticles dispersed on the conducting polymer nanofibers. In contrast to the preparation of PANI nanofibers, nanofibrillar PPy can be prepared by employing soft templates using surfactants during the chemical polymerization of pyrrole [18–20]. However, the doping state of the polymer chains becomes unpredictable if the anions of the cationic surfactants are different from those of the dopants (acid). Despite various techniques that have been developed to synthesize nanostructured PPys with various morphologies, the shape-dependent properties of PPys are rarely discussed. In a previous work, we discovered that preparation of PPy and PPy/$BaFe_{12}O_{19}$ composites by a conventional chemical oxidative polymerization yielded pure PPy films on the flask and made the ratio of

* Corresponding authors.
E-mail addresses: hanxj63@yahoo.com.cn (X. Han), hwang@lanl.gov (H.-L. Wang).

0032-3861/$ – see front matter © 2009 Elsevier Ltd. All rights reserved.
doi:10.1016/j.polymer.2009.03.005

organic to inorganic phases deviate from that desired. To resolve this problem, we suggested the application of surfactant [15].

In this paper, nanostructured PPys (spherical or fibrillar) were prepared by varying the surfactant concentrations in a surfactant-assisted oxidative polymerization route. The surfactant of choice is cetyltrimethyl ammonium chloride (CTAC) with hydrochloric acid as the dopant. The PPys undergo a spontaneous redox reaction with noble metal ions under mild aqueous conditions to produce metal nanoparticles. These nanostructured PPys exhibit morphology-dependent electrochemical properties and charge transfer mechanisms. Meanwhile, PPys are used to fabricate Au nanoparticles via chemical deposition. The effect of PPy structure on the morphologies and sizes of the Au nanoparticles is discussed.

2. Experimental

2.1. Chemicals

Pyrrole (Py, 0.968–0.971 g/cm^3), cetyltrimethyl ammonium chloride (CTAC, 98%), and chloroauric acid (Au > 47.8%) were bought from Sinopharm Chemical Reagent Co. Ltd. Ammonium persulfate (APS, 99%) was purchased from Tianjin Guangfu Fine Chemical Research Institute. All chemicals were used without further purification.

2.2. Synthesis of PPy

A typical procedure for making nanosructured PPy is described as follows: quantitative CTAC was dissolved in 0.1 M HCl, to which pyrrole monomers were then added and the mixture was mechanically stirred to form homogeneous solution. A precooled ammonium persulfate (APS) aqueous solution was poured into the above mixture to initiate the polymerization reaction. The molar ratios of monomer, oxidizing agent, and dopant were kept equal (1:1:1). The polymerization reaction was carried out in an ice-water bath for 24 h. After the reaction was completed, the resulting precipitates were centrifuged with deionized water and absolute ethanol, then left to dry in a vacuum oven at 70 °C for 24 h. The surfactant solutions were prepared by following literature [19,21] procedures with 1, 6, 12 and 18 times of critical micelle concentrations (cmc).

2.3. Chemical deposition of Au nanoparticles

PPys prepared from a surfactant concentration of 1 cmc (nanospherical, PPy1) and 12 cmc (nanofibrillar, PPy2) were used to fabricate Au nanoparticles. 1 mg PPy was dispersed in 1 ml of 1.0 mM $HAuCl_4$ solution under sonication and then the solutions were transferred to a darkroom. After reacting for 3 h, the precipitates (mixtures of PPy and metals) were centrifuged and washed with deionized water and absolute ethanol. They were then dried in a vacuum oven at 70 °C for 12 h.

2.4. Characterization

Scanning electron microscope (SEM) images of the prepared PPys and metal deposition were taken using a Hitachi S4800 scanning microscope. Raman Spectra were recorded on a Kaiser Raman spectrometer coupled to a liquid-nitrogen-cooled charge-coupled device (CCD) detector (wavelength: 785 nm). The incident laser power was kept at 1 mW with total acquisition times of 10 s. Cyclic voltammograms (CV), chronoamperometric (CA) curves and electrochemical impedance spectra (EIS) of the PPys were measured using a CHI 660 electrochemical station (USA) using

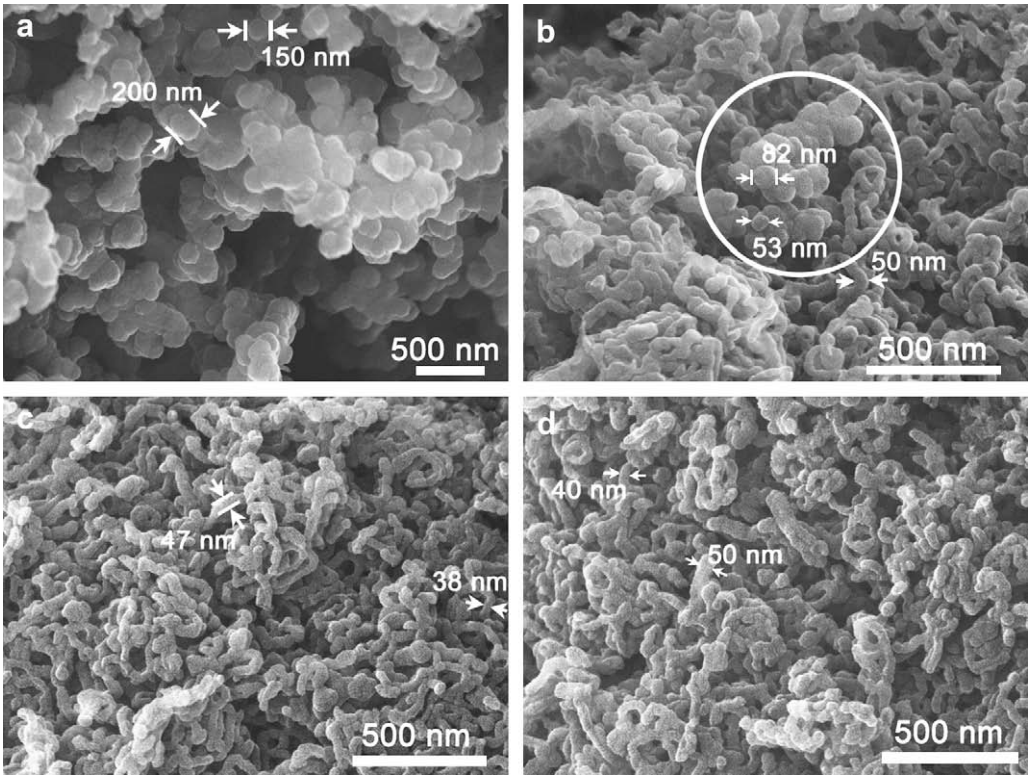

Fig. 1. SEM images of the as-prepared polypyrroles (PPys) by a surfactant-assisted oxidative polymerization route at a surfactant (cetyltrimethyl ammonium chloride, CTAC) concentration of (a) 1 cmc, (b) 6 cmc, (c) 12 cmc, and (d) 18 cmc.

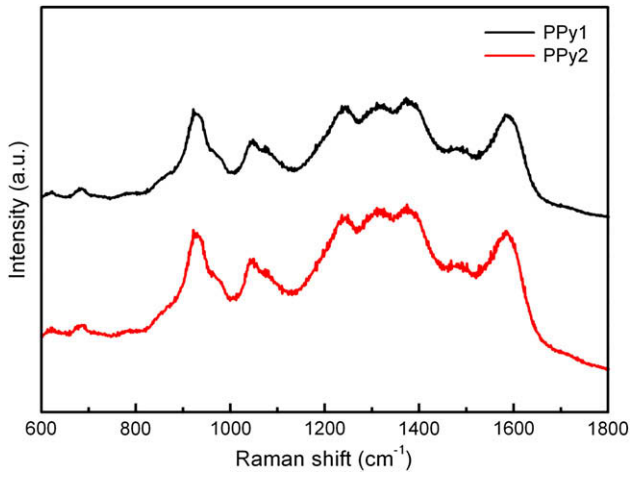

Fig. 2. Raman spectra (recorded using excitation at 785 nm) of the as-prepared PPys from different CTAC concentrations: 1 cmc (PPy1), 12 cmc (PPy2).

a glassy carbon electrode (3 mm diameter) as the working electrode, a saturated calomel electrode (SCE) as the reference electrode, and a Pt auxiliary electrode (CH Instruments, Inc.) as the counter electrode. 0.1 M HCl is used as the electrolyte. The working electrode with PPy powder is prepared as follows: 10 mg PPy was well dispersed in 0.5 ml distilled water under ultrasonication, and then the 5 μl PPy suspension was mounted onto the glassy carbon electrode. After drying in an oven at 50 °C for 1 h, a thin film of PPy was formed on the electrode surface. The crystal structures of the deposited metals were characterized using a Schimadzu XRD-6000 X-ray diffractometer with a Cu Kα radiation source ($\lambda = 1.5405$ Å, 40.0 kV, 30.0 mA).

3. Results and discussion

Our work demonstrates the use of surfactants during the polymerization reaction to yield PPys with different morphologies as a function of surfactant concentration. As shown in Fig. 1(a), interconnected spherical PPy powder with an average size of 150–200 nm was produced with a CTAC concentration of 1 cmc (0.87 mM, where spherical micelles are formed) [19,21]. When the

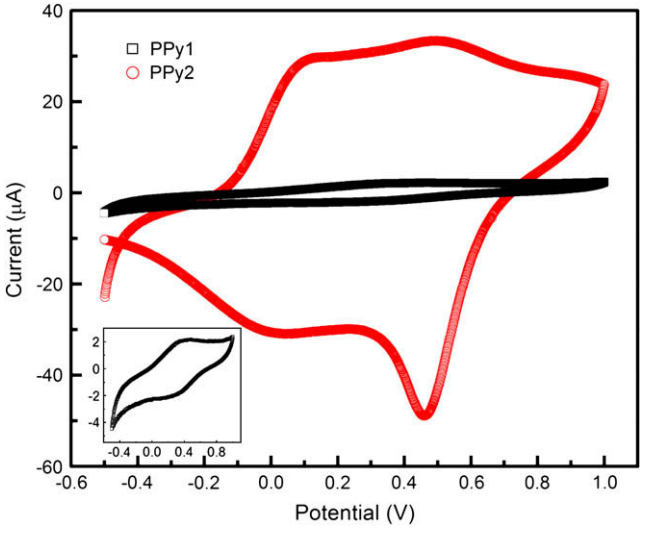

Fig. 3. Cyclic voltammograms of the as-prepared PPy from different CTAC concentrations: 1 cmc (PPy1), 12 cmc (PPy2). (*vs.* SCE, scanning rate: 10 mV s^{-1}).

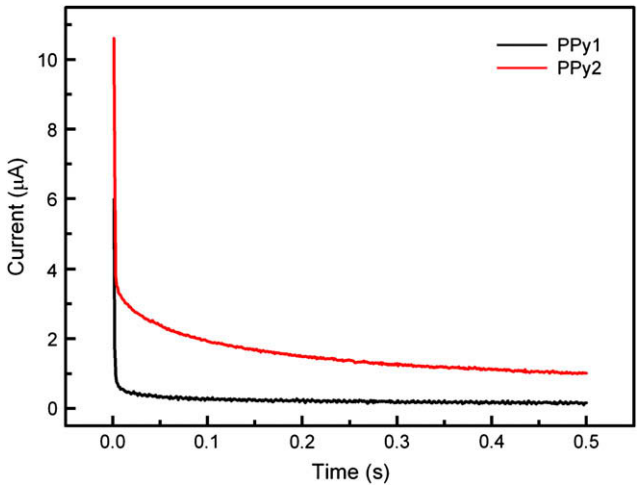

Fig. 4. Chronoamperometric curves of the as-prepared PPy from different CTAC concentrations: 1 cmc (PPy1), 12 cmc (PPy2). Open circuit voltage as initial potential, with a positive step of 10 mV.

CTAC concentration increases to 6 cmc, PPy nanofibers with an average diameter of 50 nm are obtained, which suggests the formation of some cylindrical micelles of CTAC at this concentration. However, interconnected spherical PPy nanoparticles with a size of about 50–80 nm can still be found among the nanofibers (white circle in Fig. 1(b)). Further increasing the CTAC concentration to 12 cmc results in the formation of cylindrical micelles, which leads to the formation of curled PPy nanofibers with high uniformity and narrow diameter distribution (35–50 nm). These nanofibers tend to conglomerate into interconnected and stereoscopic nanofiber networks. Furthermore, there are no noticeable differences in either morphology or size distribution for the as-prepared PPy nanofibers as we increase the CTAC concentration beyond 12 cmc (Fig. 1(d)). Similar to CTAB [19], the cationic surfactant CTAC also shows a complete transition from spherical to cylindrical micelles at a concentration greater than 12 cmc, where highly uniform PPy nanofibers with narrow diameter distributions are generated. After addition of HCl and pyrrole monomer, the cmc value of the surfactant should change as the ionic strength and pH will affect surfactant aggregation, however, it can be deduced from the prepared PPys that this influence is relatively minor. The above results suggest that the morphology of PPy, from nanospheres to nanofibers, can be controlled by varying the surfactant concentration in surfactant-assisted oxidative polymerization reactions.

The Raman spectra of spherical (PPy1) and nanofibrillar (PPy2) PPys are shown in Fig. 2, which exhibit the typical Raman bands of PPy [22–24]. A large band at 935 cm^{-1} due to ring deformation [22] is accompanied by a high-frequency band at ca. 980 cm^{-1}. Two overlapping bands centered at 1040 and 1080 cm^{-1} can be assigned as the symmetric C–H in-plane bending mode, and the band at ca. 1250 cm^{-1} corresponds to the antisymmetric C–H in-plane bending mode [22,23]. The band at 1580 cm^{-1} can be ascribed as the C=C stretching mode. Despite the fact that Raman spectra show no differences in chemical structure and functional groups, PPys with different sizes and morphology exhibit drastically different electrochemical behaviors. The cyclic voltammograms of nanospherical PPy prepared from 1 cmc CTAC (PPy1) and nanofibrillar PPy prepared from 12 cmc CTAC (PPy2) are shown in Fig. 3. Both PPy samples exhibit electrochemical activities that are manifested by a typical redox response. The difference in the redox currents, however, reflects the effective surface area that is accessible to each respective electrolyte [25]. It is apparent that nanofibrillar PPys have a higher effective surface area, a characteristic

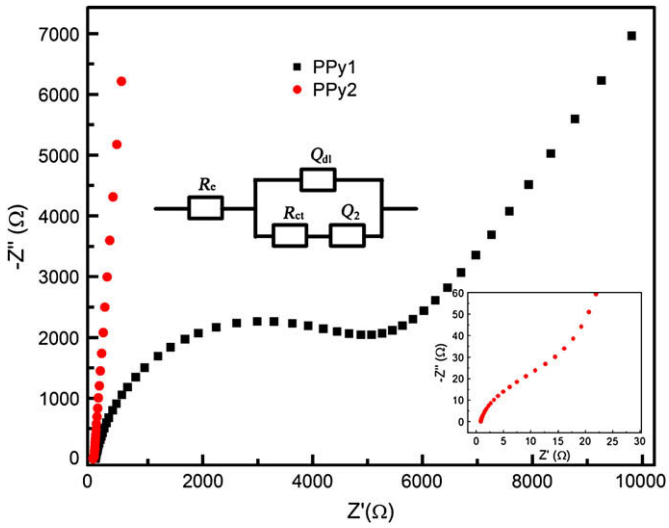

Fig. 5. Nyquist plots of the prepared PPy from different CTAC concentrations: 1 cmc (PPy1), 12 cmc (PPy2).

Table 1
Simulation results of the Nyquist curves of PPy1 and PPy2.

Sample	R_e	$Q_{dl} - Y_{dl}$	n_{dl}	R_{ct}	Q_2	n_2
PPy1	46.3	1.04×10^{-6}	0.89	3795	6.86×10^{-5}	0.46
PPy2	45.8	7.48×10^{-4}	0.95	66.39	8.28×10^{-4}	0.95

that is desirable for fabricating highly efficient/sensitive electronic and sensory devices.

During an electrochemical reaction, charge transfer between the PPys and the electrode surface needs to overcome an energy barrier. The intimate surface contact and higher surface area between the nanofibers and the electrode surface facilitate charge transfer, resulting in a higher redox current (see Fig. 3). The CV of spherical PPy (PPy1) exhibits one redox couple, consistent with previously reported results [10,26]. Interestingly, nanofibrillar PPy (PPy2) has two redox couples with oxidation potentials at 0.126 V and 0.514 V, and reduction potentials at 0.039 V and 0.462 V respectively. Splitting the curve into two peaks is assumed to be the result of two different forms of ionic species inside the polymer phase, "free" and "bound"[27]. The capability of dissipating (stabilizing) a greater number of charge species also leads to higher DC and AC conductivity, as the conductivity is directly proportional to the number of charge carriers and their mobility. This result has important implications on using this PPy nanofiber as a battery material. The chronoamperometric curves of PPy1 and PPy2 with a potential step of 10 mV are shown in Fig. 4, in which nanofibrillar PPy has a much higher current; a result that is in complete agreement with the cyclic voltammograms. By integrating the current–time curves, the redox capacities of the samples can be measured. PPy2 has a redox capacity that is ca. 10 times larger than that of the PPy1. We believe such drastic differences in current and redox capacity are mainly due to the difference in accessible surface area resulting from surface morphology.

Measurements of the frequency-dependent electrode impedance can resolve the different contributions to the electrochemical response if the time constants differ enough to allow separation. Electrochemical impedance spectra (EIS) of PPy1 and PPy2 were measured in the frequency range of 0.1–100 000 Hz and the Nyquist plots are shown in Fig. 5. The Nyquist curves are simulated by the equivalent circuit inset in Fig. 5, where R_e is the solution resistance, Q_{dl} represents the constant phase element (CPE) due to the double layer at the polymer/electrolyte interface, R_{ct} is the charge transfer resistance at this interface and Q_2 is the CPE decided by the characteristic of the polymer. The simulated results are shown in Table 1. The CPE behavior of the polymer/electrolyte interface is usually related to the details of the polymer phase structure (polymer morphology) [28]. Values of n_{dl} for PPy1 and PPy2 were found to be 0.89 and 0.95, respectively. To a first approximation, Q_{dl} can be considered as capacitance. Thus, the effective area (A) of the active materials on the electrode can be calculated from:

$$A = \frac{Y_{dl}}{C_{Hg}} \tag{1}$$

where C_{Hg} is the capacitance of pure mercury (20 μF cm^{-2}), which is a commonly used reference parameter for determining the effective area. Using this, the effective areas for PPy1 and PPy2 are 5.02×10^{-2} and 37.4 cm^2, respectively, confirming that nanofibrillar PPy has an effective surface area that is approximately three orders of magnitude higher than that of the spherical PPy. The high-frequency semicircle in the Nyquist curves represents the charge transfer resistance (R_{ct}) at the polymer/solution interface; R_{ct} of PPy1 (3795 Ω) is 57.2 times greater than that of PPy2 (66.39 Ω). It is important to note that the second constant phase element of the two samples is fundamentally different. A Warburg impedance is found for PPy1 since n_2 (0.46) is close to 0.5, indicating a semi-infinite diffusion process through the bulk to the active material. Characteristics of barrier diffusion impedance are observed for the Nyquist plot of PPy2, which means that PPy nanofibers behave more like capacitors (n_2 is 0.95 for PPy2) than PPy nanospheres. A very important perspective of these

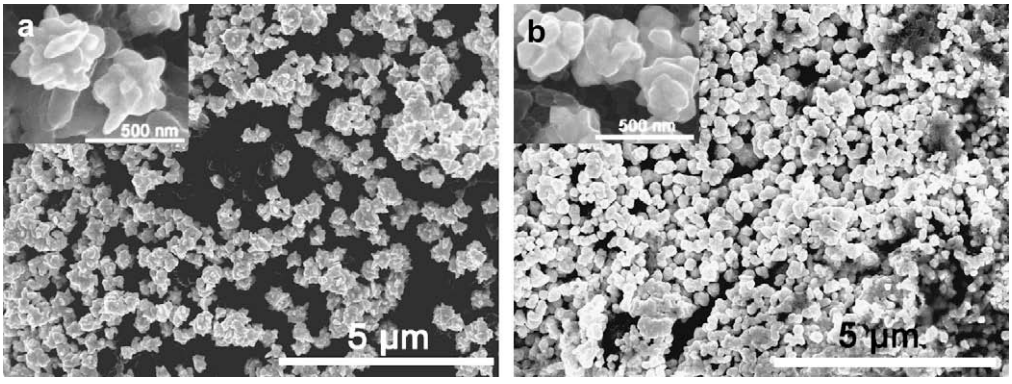

Fig. 6. SEM images of Au deposition by PPy1 (a) and PPy2 (b) in 1 mM $HAuCl_4$ solution for 3 h.

results is the potential implications toward the development of efficient batteries or capacitors. The control over electrochemical behavior resulting from their length scale and morphology also opens up opportunities in nanofiber-based sensory devices as the high surface area conducting nanofibers could facilitate the diffusion of volatile molecules which will change the PPy's conductivity.

In an attempt to better understand the morphology-dependent properties of PPys, PPy1 and PPy2 are also used for chemical deposition of metal nanoparticles from metal ion solutions. It is known that metal ions having a reduction potential higher than that of PANI can be reduced to form zero-valent metals [29–34]. However, chemical deposition of metal particles by PPy nanofibers is rarely reported [35]. If PPy serves as an electron donor, metal ions having a reduction potential higher than that of the PPy should be spontaneously reduced to form zero-valent metals ($\Delta G < 0$). Chemical deposition of Au metal was performed by dispersing 1.0 mg PPy in 1.0 ml of 1.0 mM $HAuCl_4$ aqueous solution for 3 h. Higher surface coverage of Au on PPy2 is consistent with the fact that nanofibrillar PPy has higher effective surface area (Fig. 6). Furthermore, morphological differences were discovered for the Au particles prepared from PPy1 and PPy2. Deposition of Au on PPy1 reveals a uniform star-shaped morphology. The magnified SEM image (inset) reveals submicron particulates that are in fact conglomerates of smaller Au nanosheets. In contrast, we observe highly uniformed sphere-like Au particulates in the chemical deposition by PPy2. Close examination of the particulates shows that they are composed of Au nanoparticles ($\sim$100 nm) with rice-grain shapes. The structure of the star-shaped (conglomerates of Au nanosheets) and sphere-like (conglomerates of rice-grain Au nanoparticles) particles is further validated by the XRD spectra, as shown in Fig. 7. XRD spectra reveal all four peaks that were clearly assigned to the four peaks belong to bulk Au. Moreover, the slight broadening of the XRD peaks resulting from nanoscale metal particles is consistent with the size of our Au particles.

Metal deposition through chemical reduction requires electrons to be transferred from the PPy to the metal ions. As the metal ions approach the PPy surfaces, they are reduced by PPy and form metal nuclei. In a homogeneous system, where metal ions and reducing agent are dispersed in solution, the metal nuclei serve as catalytic sites for the growth of metal structures [32]. In this work, the nuclei are formed on the PPy surfaces; therefore, morphological differences in the deposited metal nanoparticles correspond to the morphology of the PPys and may be influenced by the effective surface area accessible to the electrolytes and charge density on the PPy chains. Moreover, the presence of a more negative reduction potential in nanofibrillar PPy may produce a larger ΔG in the chemical reduction of the metal ions. In summary, the structure of the chemically deposited Au particles is directly impacted by the morphology and surface chemistry of nanostructured PPys.

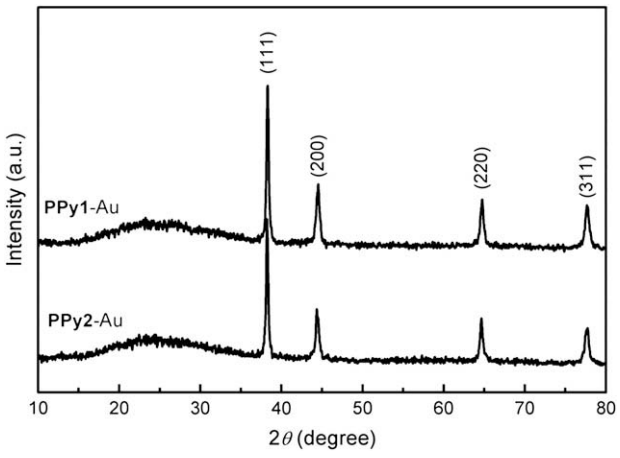

Fig. 7. X-ray diffraction patterns of Au depositions on PPy1 and PPy2.

4. Conclusions

We have demonstrated a surfactant-assisted oxidative polymerization of pyrrole to mitigate the problem of having a PPy film residue on the reaction flask which typically occurs in a conventional oxidative polymerization reaction. By controlling the surfactant concentrations and the ensuing micellar structures, nanostructured polypyrroles (PPys) with different morphologies (nanospherical or nanofibrillar) can be prepared. There is a strong correlation between the morphology of the nanostructured PPys, their electrochemical responses, and the associated charge transfer mechanisms. Nanofibrillar PPy has two redox pairs, while only one redox couple is observed for nanospherical PPy. Nanospherical PPy is shown to have a higher charge transfer resistance that is dominated by a semi-infinite diffusion process at lower frequencies, while nanofibrillar PPy behaves much more like a capacitor with a barrier diffusion process. These contrasts in electrochemical response and charge transfer mechanism, resulting from differences in surface area and surface chemistry of the conducting polymer, offer a new way to fine-tune surface energy and reduction potential that are crucial in fabricating metal particles via chemical deposition processes. The Au metals prepared from chemical reduction of $AuCl_4^-$ by PPys exhibit different morphologies from star-shaped particles comprised of Au nanosheets to sphere-like Au particulates that are actually conglomerates of rice-grain Au nanoparticles.

Acknowledgements

X. Han acknowledges financial support from the NSF of China (No. 20776032). P. Xu thanks the support from the Joint-educational Program of Chinese Scholarship Council (CSC). HLW acknowledges financial support from the National Nanotechnology Enterprise Development Center (NNEDC).

References

[1] Lieber CM. Solid State Commun 1998;107:607.
[2] Pan ZW, Dai ZR, Wang ZL. Science 2001;291:1947.
[3] Song Q, Zhang ZJ. J Am Chem Soc 2004;126:6164.
[4] Sawall DD, Villahermosa RM, Lipeles RA, Hopkins AR. Chem Mater 2004;16:1606.
[5] Li W, Wang HL. J Am Chem Soc 2004;126:2278.
[6] Li X, Wan M, Wei Y, Shen J, Chen Z. J Phys Chem B 2006;110:14623.
[7] Xu P, Han X, Jiang J, Wang X, Li X, Wen A. J Phys Chem C 2007;111:12603.
[8] Selvan ST, Spatz JP, Klok H, Möller M. Adv Mater 1998;10:132.
[9] Tian S, Liu J, Zhu T, Knoll W. Chem Mater 2004;16:4103.
[10] Bufon CCB, Vollmer J, Heinzel T. J Phys Chem B 2005;109:19191.
[11] Zhang X, Manohar SK. J Am Chem Soc 2004;126:12714.
[12] Zhang X, Goux WJ, Manohar SK. J Am Chem Soc 2004;126:4502.
[13] Huang J, Kaner RB. J Am Chem Soc 2004;126:851.
[14] Xu P, Han X, Wang C, Zhao H, Wang J, Wang X, et al. J Phys Chem B 2008;112:2775.
[15] Xu P, Han X, Wang C, Zhou D, Lv Z, Wen A, et al. J Phys Chem B 2008;112:10443.
[16] Virji S, Fowler JD, Baker CO, Huang J, Kaner RB, Weiller BH. Small 2005;1(6):624.
[17] Tseng RJ, Huang J, Ouyang J, Kaner RB, Yang Y. Nano Lett 2005;5(6):1077.
[18] Wu A, Kolla H, Manohar SK. Macromolecules 2005;38:7873.
[19] Zhang X, Zhang J, Song W, Liu Z. J Phys Chem B 2006;110:1158.
[20] Zhong W, Liu S, Chen X, Wang Y, Yang W. Macromolecules 2006;39:3224.
[21] Brinker CJ, Lu Y, Sellinger A, Fan H. Adv Mater 1999;11:579.
[22] Mikat J, Orgzall Z, Hochheimer HD. Phys Rev B 2002;65:174202.
[23] Liu YC. Langmuir 2002;18:174.
[24] Vidmond SJ, Ghaemmaghami V, Thompson M. Can J Chem 1995;73:1711.

[25] Liang L, Liu J, Windisch CF, Exarhos GJ, Lin YH. Angew Chem Int Ed 2002;41:3665.
[26] Fusalba F, Belanger D. J Phys Chem B 1999;103:9044.
[27] Levi MD, Lopez C, Vieil E, Vorotyntsev MA. Electrochim Acta 1997;42:757.
[28] Grzeszczuk M, Żabińsk-Olszak G. J Electroanal Chem 1997;427:169.
[29] Huang WS, Angelopoulos M, White JR, Park JM. Mol Cryst Liq Cryst 1990;189:227.
[30] Ting YP, Neoh KG, Kang ET, Tan KL. J Chem Tech Biotechnol 1994;59:31.
[31] Kang ET, Ting YP, Tan KL. J Appl Polym Sci 1994;12:1539.
[32] Li W, Jia QX, Wang HL. Polymer 2006;47:23.
[33] Wang HL, Li W, Jia QX, Akhadov E. Chem Mater 2007;19:520.
[34] Xu P, Han X, Wang C, Zhang B, Wang X, Wang HL. Macromol Rapid Commun 2008;29:1392.
[35] Wang H, Ding J, Lee B, Wang X, Lin T. J Mem Sci 2007;303:119.